# Design and Analysis of an Interior Continuous Magnetic Gear Box Using Finite Element Method

**Behrooz Majidi** * **and Jafar Milimonfared**

Department of Electrical Engineering
Amirkabir University of Technology, Tehran 15916, Iran
* bmx@aut.ac.ir

***Abstract*** ─ Magnetic gears offer important potential benefits compared with mechanical gears such as reduced maintenance, improved reliability, inherent overload protection, and physical isolation between the input and output shafts. This paper presents the design and analysis of a novel structure of magnet gear, which named Interior Magnetic Gear (IMG) using neodymium-iron-boron magnets for the applications in which continuous ratio of gear box is useful such as wind generators, electric vehicles and etc. The analysis is performed by Finite Element Method (FEM) to predict output torque, speed and magnetic field distribution inside the gear box. The IMG made up of an inner rotor and an outer rotor. The inner rotor is similar to the rotor of a 3 phase wound rotor induction motor and the outer rotor consists of 6 PM poles. Both the inner rotor and the outer rotor can be employed as a low/high speed rotating part. The interior arrangement of PMs result many advantage such as low torque ripple. The simulation and analytical results are in good accord.

***Index Terms*** ─ Continuous, Finite Element Method (FEM), Interior Magnetic Gear (IMG), Permanent Magnet (PM).

## I. INTRODUCTION

Mechanical gear boxes are used widely to transmit torque between separate moving parts with different speeds in various applications. For example, they are used in wind power generators to increase the rotational speed and in electric ship propulsion to decrease that. Because of the friction in mechanical gear boxes, power loss, gear noise and regular lubrication are inevitable. In the last decade magnetic gear coupling has been proposed. Magnetic gear boxes can transmit torque without any friction. They operate with the same principle as the mechanical systems where the teeth are replaced by magnet pieces. They can transform torque and speed level by interactive magnetic field between the permanent magnet pieces [1-5].

Magnetic gears offer substantial advantages compared to mechanical ones such as being maintenance free, improved reliability, minimum acoustic noise, and inherent over load protection. For example, the reduced maintenance is due to no mechanical contact and lubrication, the inherent overload protection is provided by the maximum synchronous torque, the isolation can be provided since the no mechanical contact between the inner and outer parts. At first, because of the complicated structure, low efficiency and low output torque, magnetic gear boxes in spite of some advantages have not gained much attention. In 2001, the Surface Permanent Magnet-type (SPM-type) magnetic gears has been introduced in a practical application on account of its novel design [6]. Since then, various types of magnetic gears have been proposed to develop torque density, lower torque ripple, higher ratios and efficiency [7-11]. Recent investigations focus are on implementing of continuous ratio gear boxes to be applicable for wind generators, electric vehicles and other analogous applications in which continuous ratio of gear box is essential [12-17]. Reference [18] proposes a new magnetic gear based on super conductors to achieve high torque density. In 2004-2005, in linear motors field, linear-type magnetic gears were designed [19-20]. Reference [21] proposed a new design of cycloid-type magnetic gears to achieve more torque density at high ratio. References [22-23] proposed a new type of

*Submitted On: January 18, 2014*
*Accepted On: September 28, 2014*

magnetic gear named axial-type magnetic gear. References [24-25] suggested a harmonic-type magnetic gear similar to a harmonic mechanical gear. As the coaxial magnetic gears are the most applicable type of magnetic gears, the new arrangement of PMs is applied in this type of magnetic gears. One of the most popular arrangements is Coaxial Magnetic Gear with Halbach Permanent-Magnet Arrays [26-28]. Recently, to achieve continuous ratio in gear boxes, a structure has been proposed which provides variable speed but has sophisticated structure [29].

In this paper, continuous ratio capability and simple design for manufacturing are the main goals which are analyzed by Finite Element Method (FEM) and validated by vector analytical calculation. To estimating performance of the magnetic gear, the air-gap magnetic field is computed by steady state analytical method and then compared with FEM results depicting air-gap magnetic field distribution. This adjustable continuous topology is quite suitable for many applications such as wind generators (which improves harmonic characteristics and eliminates back to back converters) and electric vehicles. This gear box can operate as a clutch and separate power from load. This advantage can make torque (speed) transmission systems very compact and simple. The operation principles of proposed magnetic gear box are presented first, and the design of this structure, which is consisted of the inner and the outer rotors is then introduced. In the next step, the proposed gear box is mathematically analyzed and its descriptive equations are derived. Finally, the validity of the obtained formulas is confirmed by simulation of proposed structure.

## II. PRINCIPLE OF OPERATION

Figure 1 shows the structure of the proposed magnetic gear box. It consists of an inner rotor with three phase windings and an outer rotor which includes PMs. Each part is made up of a steel 1010, this steel has high saturation point (almost 1.8T) which is suitable for this application. In this system, the inner rotor windings produce a rotating magnetic field with desired speed and as a result of its interaction with the outer rotor permanent magnets, outer rotor rotates [30]. It is obvious that controlling the inner rotor current frequency controls the gear box ratio, which is the main idea of this paper.

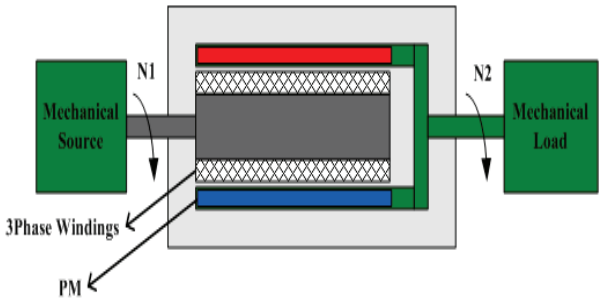


Fig. 1. Proposed topology.

It should be noted that the three-phase power is transmitted to the windings of the inner rotor through a slip ring. In other words N2=N1+Nf in which N1 is the mechanical speed of the inner rotor, Nf is the speed of the rotating magnetic field of the windings current frequency and N2 is the speed of the outer rotor.

The advantages of the purposed topology are:

1- It is possible to use this topology as a high ratio gear box which is important in gear box applications.
2- It is possible to use it as a speed regulator.
3- Possibility of controlling the output torque.
4- Inherent overload protection.
5- The proposed topology can operate as a clutch and separate the prime-mover from load.
6- Because of precision and high ratio of the proposed structure, it is possible to connect the generator output to the network (eliminating power electronic interfaces).
7- Silent working.
8- Interior arrangement reduce torque ripple.

## III. DESIGN OF THE MAGNETIC GEAR PARTS

### A. Windings and slots of the inner rotor

One of the important parts of the proposed structure is the inner rotor which its design has a great impact on the performance and behavior of the whole system. The cogging torque of the magnetic gear box arises from the interaction of permanent magnets and the inner rotor slotted structure without the applied driving current [31]. Since an oscillatory torque always induces vibration, acoustic noise, and possible resonance especially at high load and low speed, the slots of the inner rotor have been designed in order to minimize the cogging torque. Figure 2 shows the structure of the inner rotor.

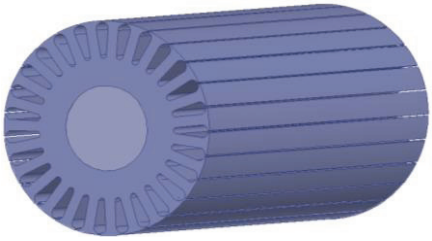

Fig. 2. 3D view of the inner rotor.

Windings type of the inner rotor is fractional slot and shorted pitch. This selection is based on evaluating of various windings performances in FEM simulation [32]. This type of the inner rotor windings improves the machine characteristics such as harmonic specifications. With proper selection of windings step, it is possible to minimize the attenuation coefficient for main frequency and maximize it for other harmonics. The inner rotor has 27 slots and its windings layout is according to Fig. 3.

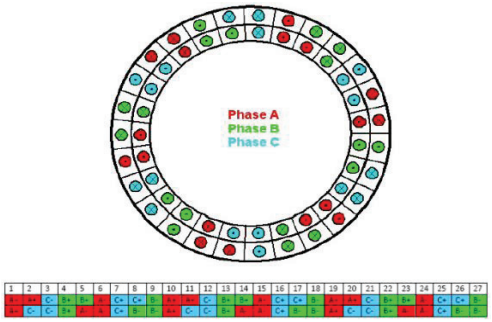


Fig. 3. Windings layout in the inner rotor.

Parameters of the inner rotor windings are presented in Table 1. In this table, q is the number of slots per pole per phase (spp), $\gamma^{oe}$ is electrical pitch angle, $K_d$ is distribution factor, $K_p$ is shortage pitch coefficient of windings and α is the slot angle.

Table 1: Inner rotor windings parameters

| Parameter | Value |
|---|---|
| q(spp) | 1.5 |
| Kd | 0.985 |
| $K_p$ | 0.998 |
| $\gamma^{oe}$ | $30^{o}$ |
| α | $13.33^{o}$ |

The implemented and simulated models of the inner rotor are shown in Fig. 4.

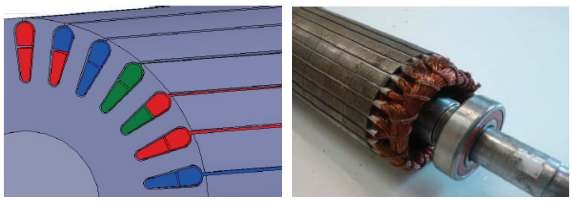

(a) (b)

Fig. 4. (a) Simulated model, and (b) implemented view of the inner rotor.

**B. Outer rotor**

According to the inner rotor structure, the outer rotor is designed and constructed whose model is shown in Fig. 5. More details of the outer rotor design are discussed in part 5. The permanent magnets are Neodymium rare earth type with grade of N35 (NdFe35).

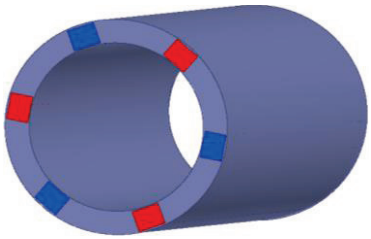

Fig. 5. Simulated model of the outer rotor.

## IV. ANALYSIS OF THE INTERIOR MAGNETIC GEAR (IMG)

The aim of this section is calculation of the output torque of the IMG which is produced by interaction of two magnetic fields, one by windings current (in the inner rotor) and the other one by permanent magnets (in the outer rotor). $F_{ri}$ is the peak value of the inner rotor windings Magneto Motive Force (MMF) and $F_{ro}$ is the peak value of the outer rotor MMF. It is obvious that output torque is equivalent of the multiplex of these fields and sinus of the angle between them as shown in Fig. 6. For calculating output torque the following assumptions has been taken into account [33]:

- The inner and outer rotors are made of material with infinite permeability.
- Air gap length is much less than average radius; there is no difference in the inner rotor surface flux with the outer rotor surface flux.
- Only the main field component of the inner and outer rotors will be taken into account.
- Because of the mechanical consideration, the air gap length (g) can't be very small.

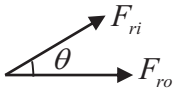


Fig. 6. Field vectors of the inner and outer rotors.

Magnitude of the resultant MMF in the air gap can be calculated as:

$$F_R = \sqrt{F_{ro}^2 + F_{ri}^2 + 2F_{ro}F_{ri}\cos\theta}. \quad (1)$$

In Eq. (1), "$\theta$" is the angle between $F_{ro}$ and $F_{ri}$.

The magnetic field intensity in the air gap $H_g$ is:

$$H_g = \frac{F_R}{g}. \quad (2)$$

Then the average of co-energy density in the air gap is:

$$W' = \frac{1}{2}\frac{\mu_0}{g^2} \times \left(\frac{1}{2}F_R{}^2\right) = \frac{1}{4}\mu_0\left(\frac{F_R}{g}\right)^2. \quad (3)$$

Eq. (1) and Eq. (3) can be combined to calculate the total co-energy in the air gap:

$$W_t' = \frac{1}{2}\frac{\mu_0}{g^2}F_R^2\left(2\pi rlg\right) = \frac{1}{2}\frac{\mu_0\pi rl}{g}F_R^2. \quad (4)$$

Considering $\theta = \frac{P}{2}\theta_m$, the output torque can be written as:

$$\begin{aligned} T_e &= \frac{\partial W_t'}{\partial\theta_m}\left(F_{ro}, F_{ri}, \theta\right) = \frac{\partial W_t'}{\partial\theta}\left(F_{ro}, F_{ri}, \theta\right)\frac{\partial\theta}{\partial\theta_m} \\ &= \frac{P}{2}\frac{\mu_0\pi rl}{g}\frac{\partial}{\partial\theta}\left(F_{ro}^2 + F_{ri}^2 + 2F_{ro}F_{ri}\cos\theta\right) \\ &= -\frac{P}{2}\frac{\mu_0\pi rl}{g}F_{ro}F_{ri}\sin\theta. \end{aligned} \quad (5)$$

Rewriting the Eq. (5) with $F_R$:

$$T_e = -\frac{P}{2}\frac{\mu_0\pi rl}{g}F_{ri}F_R\sin\delta, \quad (6)$$

by substituting:

$$F_R = gH_P = g\frac{B_P}{\mu_0}, \quad (7)$$

$$\varphi = \frac{4}{P}B_P lr \rightarrow B_P = \frac{P}{4}\frac{\varphi}{lr}, \quad (8)$$

$$F_{ri} = m\frac{2\sqrt{2}}{\pi}k_w\frac{N_{ph}I}{P}, \quad (9)$$

$$\varphi = \frac{E_{ph}}{\sqrt{2}\pi f N_{ph}k_w}, \quad (10)$$

into Eq. (6), it is possible to write it in a more useful form:

$$\begin{aligned} T_e &= \frac{\pi}{8}P^2\varphi F_{ri}\sin\delta \\ &= -\frac{\pi}{8}P^2\left(\frac{E_{ph}}{\sqrt{2}\pi f N_{ph}k_w}\right)\left(m\frac{2\sqrt{2}}{\pi}k_w\frac{N_{ph}I}{P}\right)\sin\delta \\ &= \frac{P}{4\pi f}mE_{ph}I\sin\delta = \frac{1}{\omega_m}mE_{ph}I\sin\delta. \end{aligned} \quad (11)$$

In these equations $\varphi$ is the air gap flux, $E_{Ph}$ is induced voltage per phase in the inner rotor, $N_{Ph}$ is effective turns of the inner rotor windings per phase, $K_w$ is the inner rotor windings coefficient and I is its current. Eq. (11) can be written as in below:

$$T_e = \frac{1}{\omega_m}mE_{ph}I\sin\delta = \frac{1}{\omega_m}mE_{ph}I\cos\theta, \quad (12)$$

where $\delta = \theta + 90$ in which $\theta$ is the phase angle between $E_{Ph}$ and I.

## V. SIMULATION AND EVALUATION OF THE PROPOSED GEAR BOX

In this section, the design of the proposed magnetic gear and the associated parts are presented and discussed, and finally evaluated based on the earlier-discussed issues. Table 2 summarizes the parameters of a proposed IMG.

Table 2: Specifications of a proposed IMG

| Parameter | Value | Parameter | Value |
|---|---|---|---|
| Shaft radius | 15 mm | Turns per slot layer | 33 |
| PM length | 9 mm | Number of PMs | 6 |
| PM width | 10 mm | Current density | 5 A/mm$^2$ |
| Air-gap length (g) | 0.8 mm | Steel grade | M19 |
| Inner-rotor back-iron length | 35.2 mm | Slot per pole per phase | 1.5 |
| Outer-rotor back-iron length | 10 mm | Windings type | Fractional slot, fractional pitch |
| Axial length | 140 mm | Number of slots | 27 |

It is worth noting that PM specifications cannot be chosen freely, and must be selected among the

standard ones given in Table 3.

Table 3: Approximate value of PMs specification

| Type | $B_r$ (T) | $H_c$ (kA/m) | Type | $B_r$ (T) | $H_c$ (kA/m) |
|---|---|---|---|---|---|
| N27 | 1.05 | 800 | N40 | 1.27 | 928 |
| N30 | 1.10 | 800 | N42 | 1.30 | 928 |
| N33 | 1.15 | 840 | N45 | 1.35 | 870 |
| N35 | 1.19 | 872 | N48 | 1.40 | 840 |
| N38 | 1.23 | 904 | N50 | 1.42 | 840 |

The B-H characteristic of the utilized steel (M19) is depicted in Fig. 7.

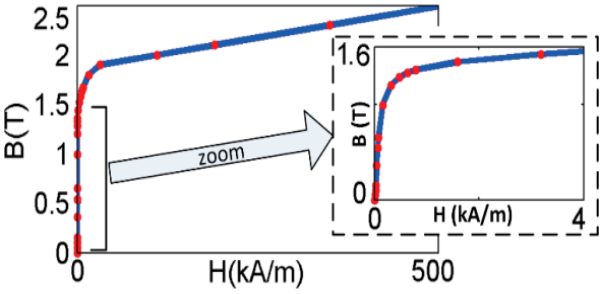


Fig. 7. B-H characteristic of the utilized steel with grade M19-29G.

Because of the mechanical considerations, the minimum air-gap length is about 0.8 mm as given in Table 2. The shaft radius also satisfies and provides us the torque transfer capability of 39 N.m. A satisfactory PM length and width are 10 mm so that the torque pulsations and back-EMF harmonics are simultaneously minimized, because of this sizing the leakage flux will be limited as well. A 2-Dimensional Time-Stepping Finite Element Method (2-D TSFEM), that its meshed regions is shown in Fig. 8, is employed to evaluate the design outcomes. It should be mentioned that the mesh size selection is critical to achieve accurate results. At first, we chose an initial mesh with relatively larger elements. Then, we made them smaller step by step until no enhancement was appeared in the accuracy of the results. So, that mesh was somewhat appropriate for the simulations since it was a trade of between the run speed and accuracy. Moreover, we paid more attention to the regions having higher flux variations; e.g., air-gap and slot areas, in which smaller elements are also adopted.

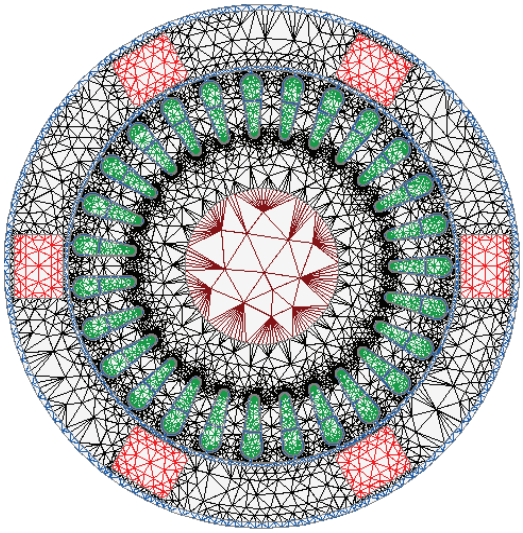

Fig. 8. Meshed regions of the FEM employed for evaluating the proposed IMG.

The proposed design also provides an appreciable demagnetization withstand capability by an appropriate field intensity ratio of $H_m/H_c=0.5$. The rotor radius is large enough to avoid saturation and the length of the outer-rotor back iron is properly designed as well. The magnetic flux density distribution within the device is shown in Fig. 9, which validates the design. This model has been used for various operating conditions to evaluate the proposed IMG behavior.

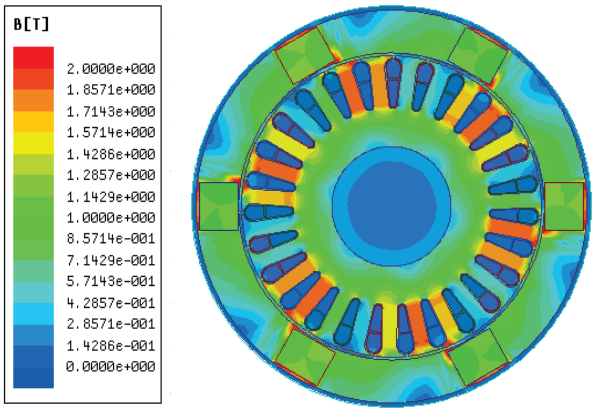


Fig. 9. Magnetic flux density distribution within the proposed IMG.

In generator mode, if the outer rotor rotates at the speed of 1000 rpm while the inner rotor is fixed, the three phase voltage induced in the windings is determined as shown in Fig. 10. It is seen that the voltage waveforms are sinusoidal that finally simplifies the drive system, all of which originates from the proper machine design; e.g., the inner-rotor windings and slots, and PMs.

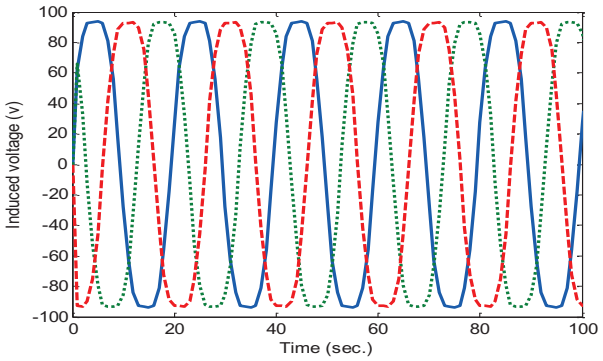


Fig. 10. Induced voltage in the inner rotor windings.

In Fig. 11, gear box torque and speed with 20 N.m loading are shown. Since the windings current frequency is 50 Hz, the rotating magnetic field is 1000 rpm, and the initial mechanical speed of the inner rotor is 500 rpm; therefore, the speed of the outer rotor is 1500 rpm, i.e., 1000+500 rpm. It is observed that the gear box has been stabilized in desired values. Since in the generator mode the back-EMF amplitude was 96 volt, while the applied voltage is on the inner rotor terminals, to compensate for the voltage drop on the windings, the applied voltage is set to $V_{peak}$=105 volt, i.e., a little higher. This voltage is transmitted to the windings of the inner rotor through a slip ring.

At this point, by simulating the IMG without the outer rotor permanent magnets, it is possible to plot the air gap flux density and flux linkage waveforms (Fig. 12) and evaluate Eqs. (8) and (10). Issued from the machine having the specifications given in Table 2, we achieve: $\varphi = 0.000442\ wb$, $\lambda = 0.129\ wb$ and the air gap flux density is B=0.121 T. Finally, by knowing the phase difference between voltage and current in the inner rotor windings, an output torque of 20.84 N.m is obtained. It is worth noting that the presented equations well describe the gear box behavior in steady state operation and are in good agreement with those extracted from simulations.

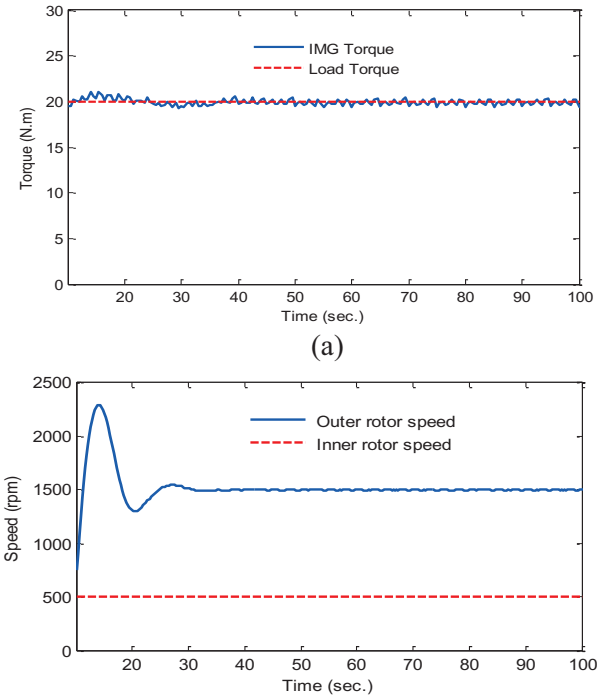


Fig. 11. (a) Output torque, and (b) speed of the IMG.

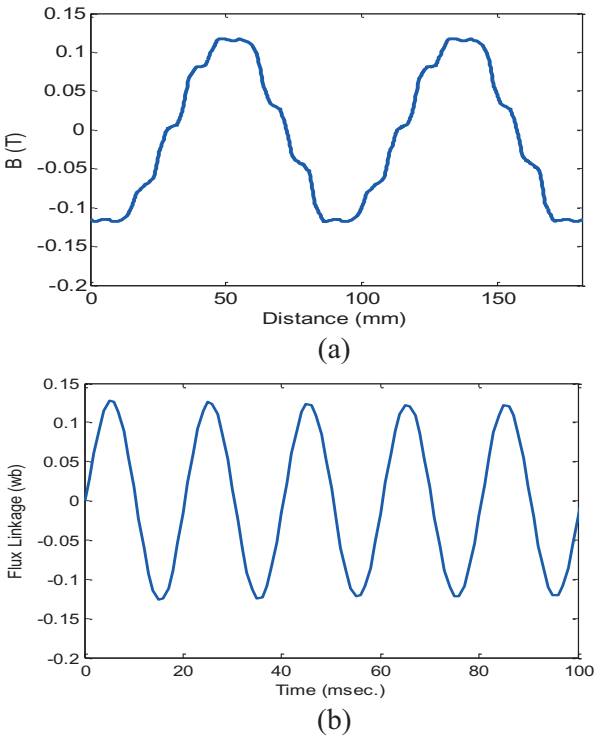


Fig. 12. (a) Flux density, and (b) flux linkage waveforms in the air gap caused by the inner rotor windings.

## VI. CONCLUSION

In this paper, the analysis and simulation of a novel structure of magnet gear, which named interior magnetic gear using neodymium-iron-boron magnets is carried out in which can be employed in wind generators, electric vehicles, etc., wherein a continuous ratio of gear box is required. To this end, finite elements analyses are performed to predict the main characteristics of the device including output torque, speed and magnetic field distributions. Both the inner and the outer rotors can be exploited as a low/high speed rotating part by controlling the frequency of the inner rotor windings current. The output torque and other parameters such as B are evaluated in the steady state condition using vector analysis. Simulation results are also in good agreement with theoretical analysis.

### REFERENCES


[1] K. Tsurumoto and S. Kikushi, "A new magnetic gear using permanent magnet," *IEEE Trans. Magn.*, vol. 23, no. 5, pp. 3622–3624, 1987.

[2] D.R. Huang, Y.D.Yao, S.M. Lin and S.J.Wang, "The Radial Magnetic Couplings between Magnetic Gears," *IEEE Trans. Magn.*, vol. 31, no. 6, pp. 17-21, Nov. 1995.

[3] Y.D.Yao, D.H.Huang, S.M. Lin and S.J.Wang, "Theoretical Computations of the Magnetic Coupling between Magnetic Gears," *IEEE Trans. Magn.*, vol. 32, no. 3, pp. 710-713, May 1996.

[4] A. Sarikhani , O. A. Mohammed, "Coupled electromagnetic field computation with external circuit for the evaluation the performance of electric motor designs," *ACES Journal*, vol. 26, no. 12, 2011.

[5] E. Schmidt, M. Hofer, "Application of the sliding surface method with 3D finite element analyses of a hybrid magnetic bearing," *ACES Conference, Low-Frequency Computational Electromagcs*, 2009.

[6] K. Atallah and D. Howe, "A novel high-performance magnetic gear," *IEEE Trans. Magn.*, vol. 37, no. 4, pp. 2844–2846, July. 2001.

[7] P. O. Rasmussen, T. O. Andersen, F. T. Jørgensen, and O. Nielsen, "Development of a high-performance magnetic gear," *IEEE Trans. Ind. Appl.,* vol. 41, no. 3, pp. 764–770, May/Jun. 2005.

[8] C. Huang, M. Tsai, D. G. Dorrell, and B. Lin, "Development of a magnetic planetary gearbox," *IEEE Trans. Magn.*, vol. 44, no. 3, pp. 403–412, Mar. 2008.

[9] L.L. Wang, J.X. Shen, P.C.K. Luk, W.Z. Fei, C.F. Wang and H. Hao, "Development of a Magnetic-Geared Permanent-Magnet Brushless Motor," *IEEE Trans. Magn.*, vol. 45, no. 10, pp. 4578–4581, Oct. 2009.

[10] N. Niguchi and K. Hirata, "Torque-Speed Characteristics Analysis of a Magnetic-Geared Motor Using Finite Element Method Coupled With Vector Control," *IEEE Trans. Magn.*, vol. 49, no. 5, pp. 2401–2404, 2013.

[11] P.O. Rasmussen, T.V. Frandsen, K.K. Jensen and K. Jessen, "Experimental Evaluation of a Motor-Integrated Permanent-Magnet Gear," *IEEE Trans. Ind. Appl.*, vol. 49, no. 2, pp. 850–859, 2013.

[12] L. Jian, K.T. Chau and J.Z. Jiang, "A Magnetic-Geared Outer-Rotor Permanent-Magnet Brushless Machine for Wind Power Generation*," IEEE Trans. Ind. Appl.,* vol. 45, no. 3, pp. 954–962, Nov. 2009.

[13] K.T. Chau, D. Zhang, J.Z. Jiang, Ch. Liu and Y. Zhang, "Design of a Magnetic-Geared Outer-Rotor Permanent-Magnet Brushless Motor for Electric Vehicles," *IEEE Trans. Ind. Appl.*, vol. 43, no. 6, pp. 2504–2506, Feb. 2007.

[14] M. Aubertin, A. Tounzi and Y.L. Menach, "Study of an Electromagnetic Gearbox Involving Two Permanent Magnet Synchronous Machines Using 3-D-FEM," *IEEE Trans. Ind. Appl.*, vol. 44, no. 11, pp. 81–84, Nov. 2008.

[15] Z. Haznadar, Z. Stih, S. Berberovic, G. Manenica, "The application of the finite element method in design of electric motors," *ACES Journal*, vol. 9, no. 2, 1994.

[16] O. A. Mohammed, S. Ganu, N. Abed, S. Liu, Z. Liu, "High Frequency Phase Variable Model of Electric Machines from Electromagnetic Field Computation," *ACES Journal*, vol. 22, no. 1, 2007.

[17] H. Torkaman, N. Arbab, H. Karim, E. Afjei, "Fundamental and Magnetic Force Analysis of an External Rotor Switched Reluctance Motor," *ACES Journal*, vol. 26, no. 10, 2011.

[18] M. Okano, K. Tsurumoto, Sh. Togo, N. Tamada and Sh. Fuchino, "Characteristics of the magnetic gear using a bulk high-Tc superconductor," *IEEE Trans. Appl. Supercond.,* vol. 12, no. 1, pp. 979–983, March. 2002.

[19] K. Atallah, J. Wang, and D. Howe, "A high-performance linear magnetic gear," *J. Appl. Phys.,* vol. 97, pp. 10N516-1–10N516-3, 2005.

[20] P. Zheng, B. Yu, H. Yan, Y. Sui, J. Bai, P. Wang, "Electromagnetic Analysis of a Novel Cylindrical Transverse-Flux Permanent-Magnet Linear Machine," *ACES Journal*, vol. 28, no. 9, 2013.

[20] F.T. Jorgensen, T.O. Andersen and P.O. Rasmussen, "The Cycloid Permanent Magnetic Gear," *IEEE Trans. Ind. Appl.,* vol. 44, no. 6, pp. 1659–1665, Nov. 2008.

[21] S. Mezani, K. Atallah, and D. Howe, "A high-performance axial-field magnetic gear," *J. Appl. Phys.,* vol. 99, pp. 08R303-1–08R303-3, 2006.

[22] V.M. Acharya, J.Z. Bird and M. Calvin, "A Flux Focusing Axial Magnetic Gear," *IEEE Trans. Magn.*, vol. 49, no. 7, pp. 4092–4095, 2013.

[24] J. Rens, R. Clark, S. Calverley, K. Atallah and D. Howe, "Design, analysis and realization of a novel magnetic harmonic gear," *18th International Conference on Electrical Machines (ICEM)*, pp. 1-4, 2009.

[25] J. Rens, K. Atallah, S.D. Calverley and D. Howe, "A Novel Magnetic Harmonic Gear," *IEEE Trans. Ind. Appl.,* vol. 46, no. 1, pp. 206–212, Jan./Feb. 2010.

[26] Z. Q. Zhu and D. Howe, "Halbach permanent magnet machines and applications: a review," *Inst. Electr. Eng. Proc. Electr. Power Appl.,* vol. 148, no. 4, pp. 299–308, Jul. 2001.

[27] J. Choi and J. Yoo, "Design of a Halbach magnet array based on optimization techniques," *IEEE Trans. Magn.*, vol. 44, no. 10, pp. 2361–2366, Oct. 2008.

[28] L. Jian and K.T. Chau, "A Coaxial Magnetic Gear With Halbach Permanent-Magnet Arrays," *IEEE Trans. Energy Convers.*, vol. 25, no. 2, pp. 319–328, June. 2010.

[29] L. Shah, A. Cruden and B.W. Williams, "A Variable Speed Magnetic Gear Box Using Contra-Rotating Input Shafts," *IEEE Trans. Magn.*,vol. 47, no. 2, pp. 431–438, Feb. 2011.

[30] P. Vas, "Sensorless Vector and Direct Torque Control," Oxford Press, New York, 1998.

[31] N. Niguchi and K. Hirata, "Cogging Torque Analysis of Magnetic Gear," *IEEE Trans. Ind. Electron.,* vol. 59, no. 5, pp. 2189–2197, 2012.

[32] H. Lesani, "Windings of Electric Machinery," 3nd edition," Daneshofan Press, Tehran, Iran1995.

[33] G.R. Slemon, "Electric Machines and Drives," Addison-Wesley Publication Company, 1992.

**Behrooz Majidi** was born in Isfahan, Iran. He received his M.Sc degree in electrical engineering from Amirkabir University of Technology (Tehran Polytechnic), Tehran, Iran. He is currently Ph.D student at Amirkabir University of Technology (AUT). His research interests include power electronics, electrical machines and variable speed drives.

**Jafar milimonfared** received the B.Sc. Degree in electrical engineering from Amirkabir University of Technology, and both the M.Sc. and Ph.D. degrees from Paris VI University, Paris, France in 1981 and 1984 respectively. Dr. Milimonfared joined Amirkabir University of Technology as an assistant professor in 1984 where he is now a professor of electrical engineering. From 1990 to 1993 and from 1997 to 2005, he was the deputy of Ministry of Science, Research and Technology in Iran. He is now head of Iran Mechatronics Society. His research interests include electrical machines design and analysis, power electronic and variable speed drives.